

# VEnvision3D: A Synthetic Perception Dataset for 3D Multi-Task Model Research

Jiahao Zhou<sup>1†</sup>, Chen Long<sup>2†</sup>, Yue Xie<sup>2</sup>, Jialiang Wang<sup>1</sup>, Boheng Li<sup>3</sup>,  
Haiping Wang<sup>2</sup>, Zhe Chen<sup>2\*</sup>, and Zhen Dong<sup>2</sup>

<sup>1</sup> School of Remote Sensing and Information Engineering, Wuhan University, China

<sup>2</sup> State Key Laboratory of Information Engineering in Surveying, Mapping and Remote Sensing, Wuhan University, China

<sup>3</sup> Key Laboratory of Aerospace Information Security and Trusted Computing, Ministry of Education, School of Cyber Science and Engineering, Wuhan University, China

<sup>†</sup> Equal contribution \* Corresponding author.

**Abstract.** Developing a unified multi-task foundation model has become a critical challenge in computer vision research. In the current field of 3D computer vision, most datasets only focus on single task, which complicates the concurrent training requirements of various downstream tasks. In this paper, we introduce VEnvision3D, a large 3D synthetic perception dataset for multi-task learning, including depth completion, segmentation, upsampling, place recognition, and 3D reconstruction. Since the data for each task is collected in the same environmental domain, sub-tasks are inherently aligned in terms of the utilized data. Therefore, such a unique attribute can assist in exploring the potential for the multi-task model and even the foundation model without separate training methods. Meanwhile, capitalizing on the advantage of virtual environments being freely editable, we implement some novel settings such as simulating temporal changes in the environment and sampling point clouds on model surfaces. These characteristics enable us to present several new benchmarks. We also perform extensive studies on multi-task end-to-end models, revealing new observations, challenges, and opportunities for future research. Our dataset and code will be open-sourced upon acceptance.

**Keywords:** 3D computer vision · Datasets and evaluation · Point cloud understanding · Multi-task learning · Environment simulation

## 1 Introduction

The development of AI models has made many novel tasks possible. In recent years, vision foundation models [6] (trained on a vast quantity of data at scale such that they can be adapted to a wide range of downstream tasks) have once again sparked transformative revolutions across diverse industries. Examples include CLIP [46] and SAM [31] in 2D computer vision, as well as UniAD [27]

in autonomous driving. *Multi-task, unified, end-to-end* frameworks have become the new direction for the vision foundation model.

The development of these models has benefited from the emergence of large-scale, high-quality data [69], such as the widely successful ImageNet [12]. Thanks to the availability of large-scale 2D image datasets and relatively small domain shifts between images [68], the development of the foundation model in 2D computer vision has become relatively mature. However, due to a relatively late start, we lack a large number of available datasets in 3D computer vision. As shown in Fig. 1, with a significantly smaller quantity of datasets compared to datasets in the 2D domain, some mainstream datasets also have much smaller scales [4, 9, 12, 17, 36, 37].

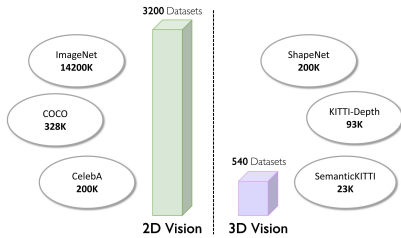


**Fig. 1:** A comparison between dataset quantities in 2D and 3D vision and the data volume of classic datasets. The statistic data is from the Papers With Code [1] website.

	Dataset	Cities	Task				
			Dep.	Ups.	Seg.	Recg.	Recs.
Real-world	KITTI [17]	1	✓				✓
	SemanticKITTI [4]	1			✓		
	ShapeNet [9]	object		✓	✓		✓
	Oxford RobotCar [39]	1				✓	✓
	S3DIS [3]	indoor			✓		
Synthetic	SynthCity [18]	1			✓		
	STPLS3D [10]	aerial			✓		
	KITTI-CARLA [13]	8	✓		✓		✓
	AIODrive [60]	8	✓		✓		
	SHIFT [52]	8	✓				✓
	VEnvision3D (Ours)	11	✓	✓	✓	✓	✓

**Table 1:** Comparison of supported tasks of existing 3D point cloud datasets. VEnvision3D is the only dataset that simultaneously supports depth completion(Dep.), segmentation(Seg.), upsampling(Ups.), place recognition(Recg.), and 3D reconstruction(Recs.) in the same environmental domain.

With only a handful of datasets available to 3D vision researchers, parameter differences between 3D sensors lead to larger domain gap than 2D images, making the situation even more unpromising. This large gap further allows a dataset to be used for only one task for which it was designed. For example, the SemanticKITTI [4] dataset provides large-scale annotated point clouds for segmentation, but the fixed collection route makes it unable to be used for place recognition task. Such a situation forces us to train multiple networks separately on different datasets, which not only affects the efficiency and accuracy of multi-task models but also limits the exploration of inter-task relationships [57].

A dataset collected within the same environmental domain is required for investigating the relationships among sub-tasks, which can offer fresh insights into the development of 3D vision multi-task models. In this paper, we introduce VEnvision3D dataset, facilitating the exploration of multi-task models and the

relationships between tasks in the field of 3D Vision, including depth completion, segmentation, upsampling, place recognition, and 3D reconstruction. Using CARLA Simulator [15], we divide the dataset into several subsets by specific task. To unify the data collection of multiple sub-tasks, it necessitates a meticulously designed distribution of sensors, a setup that presents more challenges compared to collecting single data types. The advantage of virtual environments being freely editable makes this possible. Concurrently, in the process of exploration, we also implement features that were previously difficult to realize in the real world, such as simulating temporal changes in the environment and sampling point clouds on model surfaces. We manifest data, which in real life incurs high costs, within virtual worlds, thereby providing preliminary data support for more cutting-edge research in the future. This expands the range of scenarios and variation factors for evaluating algorithm performance, enabling a more comprehensive exploration of their robustness and adaptability.

Additionally, we conduct experiments to investigate the mutually beneficial relationships among specific tasks. To explore this initially, we design an multi-task end-to-end framework to leverage the features between different sub-tasks, thereby achieving semantic segmentation and upsampling concurrently. The experimental results tentatively reveal that this mutually beneficial relationship can improve the accuracy of sub-tasks. Beyond the scope of multi-task model development, we believe that our dataset can assist researchers in exploring the potential for unified models. Thus, we can offer a platform that fosters innovation for researchers (See Fig. 2), unify the target tasks within the field of 3D Vision, and ultimately achieve a *foundation model of future-oriented artificial general intelligence*.

The main contributions of our work are summarized as follows:

- We introduce the VEnvision3D dataset, the first synthetic dataset that allows validation of multiple tasks within the same environmental domain.
- The data collected in virtual environments yields novel attributes that are difficult to acquire in real-world situations, thereby providing new challenging benchmarks.
- Using our dataset, we design a multi-task end-to-end network to demonstrate the mutual benefits among two different tasks, highlighting the dataset’s versatility and potential to advance future research.

## 2 Related Works

Numerous 3D datasets have been proposed in the past. However, they often exhibit limitations by being restricted to a single functionality. Tab. 1 shows the functionalities provided by current mainstream datasets. We introduce the classic 3D perception datasets as follows:

### 2.1 Single-task Dataset

**Depth Completion.** Currently, datasets for depth completion tasks are relatively scarce. KITTI DC [54] is a widely used large-scale outdoor dataset that

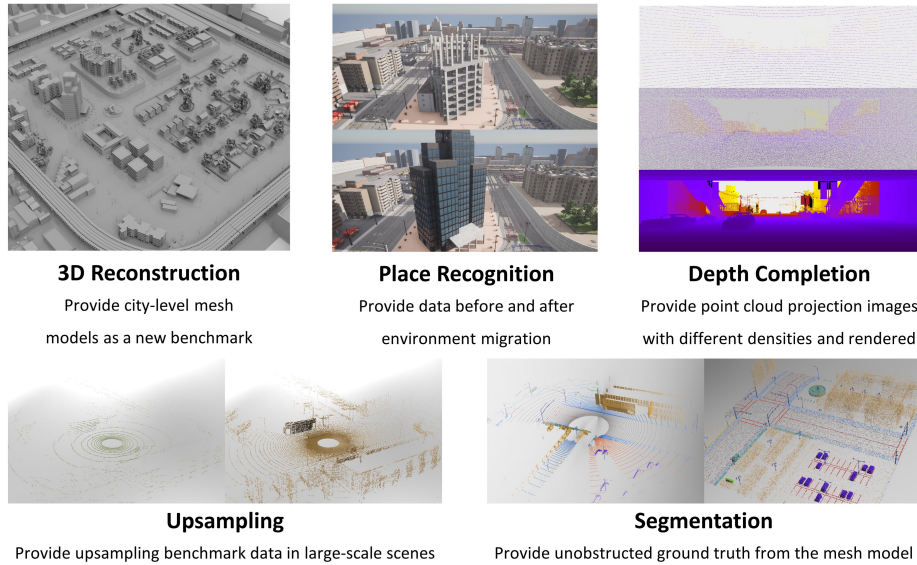


**Fig. 2:** The distinctive features of VEnvision3D dataset. Taking advantage of freely editable virtual environments, we implement many novel settings, such as the stacking of sensors, the generation of annotated city mesh models, and the simulation of environmental changes. These attributes enable us to realize multi-task functionalities and various types of data that are challenging to achieve in the real world.

contains over 93,000 semi-dense depth maps with the corresponding raw sparse LiDAR scans and RGB images [23]. The DenseLivox [66] dataset is collected with much denser depth maps than KITTI. DeepLiDAR [45] provides a synthetic dataset generated by the CARLA Simulator [15]. In comparison, our dataset provides accurate ground truth depth obtained through rendering and point cloud projected image with varying densities in the same frame.

**Upsampling.** There are various point cloud datasets [5, 9, 56, 61] used to evaluate the performance of point cloud upsampling algorithms. For object-level upsampling tasks, researchers usually downsample the ground truth as the input. Some researchers choose to build their dataset for training and testing of point cloud upsampling models [33, 43, 44, 64, 65]. Compared to ours, these datasets do not provide data collected in large-scale outdoor scenes. For the first time, we have achieved point clouds of natively varying densities at the sensor level.

**Segmentation.** For real-world datasets, SemanticKITTI [4] provides point-wise annotated point clouds. Recently, several similar vehicle-mounted outdoor scene datasets [47, 50, 58] with richer classes have been released. Besides, large-scale point clouds can be obtained through airborne LiDAR scanning [51, 63, 71] or reconstruction by photogrammetry [7, 25, 34]. Semantic3D [19] employs terrestrial LiDAR to capture outdoor scenes. S3DIS [3] utilizes depth cameras to capture indoor data, resulting in denser annotated data. For synthetic datasets, SynthCity [18] is the pioneering synthetic point cloud dataset that utilizes the Blensor



plugin in Blender to simulate LiDAR scanning. Paris-CARLA-3D [14] consists of real-world point clouds and synthesized point clouds, both annotated with the same categories, enabling exploration of domain transfer. SynLiDAR [62] is developed using the UE4 engine for the same motivation. STPLS3D [10] employs a 3D scene generation engine to synthesize virtual scenes, using a UAV simulator for photogrammetry and generating labeled point clouds. In comparison to these datasets, we simultaneously provide annotated point clouds obtained from scanning and the mesh model.

**Place Recognition.** There are currently a limited number of large-scale place recognition datasets available. Oxford RobotCar [39] and Mulran [29] are created using a LiDAR sensor mounted on a car that repeatedly drives through each region at different times. Our dataset simulates migration and changes in the environment to better explore the algorithm’s robustness.

**3D Reconstruction.** LiDAR-based SLAM has become a widely adopted method for 3D reconstruction. KITTI Odometry [17] is now the most popular benchmark for odometry evaluation. The NCLT dataset [8] comprises 27 extended sequences captured by Segway platforms. The UrbanNav dataset [21] offers a challenging data source for advancing the study of accurate and robust positioning in urban canyons. Our dataset includes city-level mesh models, enabling the development of novel benchmark methods.

While the aforementioned datasets have achieved commendable outcomes within their respective domains, it is imperative to acknowledge the profound discrepancies among 3D sensors (including brand, frequency, channels, and the number of emission points), which lead to significant domain shifts among these datasets. This necessitates individual training on each dataset, further complicating the integration of networks for various sub-tasks. There is a pressing need for a multi-task dataset that would enable researchers to design a multi-task framework in a singular effort.

## 2.2 Multi-task Dataset

Recently, some synthetic datasets with multiple sensors have been released. KITTI-CARLA [13] utilizes sensors identical to those in the KITTI dataset within a virtual environment. AIODrive [60] is generated with a specific focus on high-density and long-range LiDAR datasets. SHIFT [52] features a comprehensive sensor suite and annotations, enabling the investigation of performance degradation in perception systems as domain shift increases. These datasets are collected exclusively through CARLA.

However, these datasets merely utilize combinations of multiple sensors to fulfill multi-task requirements, with a predominant focus on 2D vision. They achieve multi-task capabilities by providing images annotated with different information. In 3D vision, sub-tasks are delineated with greater specificity and cannot be simply represented through images. This necessitates more meticulous design efforts to develop datasets capable of satisfying the requirements of multiple sub-tasks. Our dataset successfully provides the necessary data for a

variety of 3D vision sub-tasks within the same environmental domain. Moreover, leveraging the advantages of virtual environments, we have collected many forms of data that are challenging to obtain in the real world, offering more solid support for 3D multi-task learning.

### 3 VEnvision3D Dataset

In order to make our dataset available for different sub-tasks in the same frame, we design a data acquisition plan capable of accommodating multiple sub-tasks. Specific data details are presented in Tab. 2, the sensor setup is illustrated in Fig. 3, and the parameters of the sensors are listed in Tab. 3. VEnvision3D has more than 140,000 fully annotated frames, occupies more than 2,500 GB, and has a total of 13 scene variations ranging from urban to rural. Different sub-tasks can share the same frame. We additionally provide city models and semantic-annotated point clouds sampled from their surfaces.

Function	Format	Brief Description
Depth Completion	KITTI DC [54]	16/32/64/128-channel LiDAR projected image; monocular RGB image; rendered depth ground truth.
Upsampling	-	16/32/64/128-channel LiDAR scan.
Segmentation	SemanticKITTI [4]	16/32/64/128-channel LiDAR scan with semantic & instance label. Provide semantic-annotated point clouds sampled from the city mesh model.
Place Recognition	Oxford RobotCar [39]	Monocular RGB image; rendered depth image; 64-channel LiDAR scan with pose and location. Four partially overlapping scanning routes collected before and after environmental migration.
3D Reconstruction	KITTI Odometry [17]	Stereo RGB image; 64-channel LiDAR scan with pose and location. Provide city mesh models as ground truth.

**Table 2:** We organize the format of VEnvision3D according to mainstream standards. This table includes the data required for each sub-task. We can facilitate multi-task learning by providing data for different tasks in the same frame.

#### 3.1 Data Collection and Annotation

We employ LiDAR with different channel count, RGB camera, Depth camera and GNSS/IMU for data collection purposes. To enhance the realism of the LiDAR

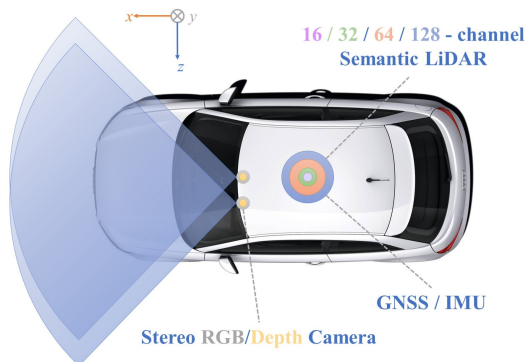


**Fig. 3:** The vehicle system and the sensor layout. We successfully stack LiDARs with different channel count at the same location to simulate point clouds of different densities at the sensor level, and the data are automatically annotated. The point clouds generated by LiDAR sensors share the exact same coordinate system and do not produce mutual occlusions.

point clouds, we manually add noise on point clouds. A selection of points is randomly perturbed along the laser ray’s direction, introducing noisy distance measurements. Taking advantage of the fact that virtual environments can be freely edited, we implement stacking of LiDAR sensors at the same location, generating point clouds that do not obscure each other and share exactly the same coordinate system. Thus we realize the collection of point clouds with different densities at the sensor level, which is the main reason why our dataset can help multi-task learning.

We allow the vehicle to follow random routes in the city map and simulate real traffic conditions in order to collect data in different scenarios. These city maps vary in size, with the largest covering 10,000 hectares and encompassing a range of scenes from urban to rural, and from streets to highways. The screenshots can be found in the supplementary materials. Note that for sub-tasks such as the 3D reconstruction and place recognition, which require fixed routes, we design several separate routes that can fulfill the task requirements. These routes overlap with the previously random ones and can also meet the requirements of other types of sub-tasks.

Thanks to the advantages of virtual environments, data annotation can be automatically performed. We provide instance and semantic segmentation labels on 28 classes and the real depth map generated by the renderer. We also obtain semantic-labeled point clouds through Monte Carlo sampling [20] from the city model, providing a new benchmark for scene-level completion, 3D reconstruction, and semantic segmentation tasks.

In response to contemporary point cloud processing research, the dataset is categorized based on various functionalities, including depth completion, segmentation, upsampling, place recognition, and 3D reconstruction. This approach

Sensor	Parameters
LiDAR	16/32/64/128-channel, 360° horizontal FoV, $-25^\circ$ to $30^\circ$ vertical FoV, 10Hz frequency, $\leq 120\text{m}$ range. With manually added noise.
RGB Camera	Resolution of $1216 \times 352$ , FoV of $90^\circ$ , Aperture of $f/1.4$ . With post-process effects.
Depth Camera	Same as RGB Camera.
GNSS/IMU	10Hz frequency.

**Table 3:** Sensor parameter settings. We meticulously configure our setup in accordance with the parameters of KITTI [17] sensors, and added noise and post-effects to ensure the realism of the data, aiming to minimize domain shift.

facilitates ease of use and enables the exploration of connections between different tasks.

### 3.2 Unique Features

**Different density data in the same frame.** In real-world scenarios, it is challenging to obtain data with varying point densities within a single frame due to the limited availability of LiDAR in vehicles. However, in our virtual environment, we strategically place LiDAR with different channel counts (16/32/64/128 channels) at the same location. This unique configuration enables us to deliver, for the first time, scene-level point clouds with multiple densities in an upsampling task at sensor level. The exploration of scene-level upsampling methods is crucial for the future development of intelligent point cloud processing. Additionally, we provide point clouds with varying densities for both depth completion and semantic segmentation tasks. These can be used to assess the algorithm’s robustness to density changes and for domain adaptation studies.

**Surface sampling from city-level model.** The existing scene-level data is obtained through LiDAR measurements, inevitably leading to the occurrence of obstructions during the collection process, making it challenging to capture the complete scene. To overcome this issue, we employ Monte Carlo Sampling to obtain point clouds and labels from the city mesh model’s surface in our dataset. Subsequently, we divide the entire point cloud into blocks of  $100\text{m} \times 120\text{m}$  (consistent with the LiDAR detection distance), with a cropping interval of 6m. This approach ensures that the blocks simulate an unobstructed effect. By adopting this method, we aim to facilitate the exploration of techniques for scene-level completion of point clouds, while previous research primarily concentrated on completing individual objects. We also believe that a city-level model can introduce innovative evaluation methods for city-scale 3D reconstruction.

**Simulate migration changes in environments.** Traditional datasets are typically obtained through a one-time acquisition process, which fails to account for temporal environmental variations such as the seasonal decay of vegetation

and the evolution of construction projects. Environmental changes are crucial for the development of adaptive algorithms, yet acquiring longitudinal real-world datasets that encompass these changes is a formidable challenge, often necessitating years of data collection. To address this gap, we use the virtual environment to simulate the construction of buildings by selectively editing existing structures. We design four routes, including repetitive paths and closures. Vehicles traverse these routes before and after the simulated environmental migration, allowing us to collect datasets reflecting different environmental parameters. We envisage that such an attribute can empower researchers to more thoroughly investigate the influence of environmental changes on place recognition algorithms.

## 4 Baseline Experiments

In this section, we test five sub-tasks provided by VEnvision3D using the current mainstream methods. For fair comparison, we faithfully follow the experimental settings of each baseline in the original publication. From the experimental result, we found the positive impact of varying point cloud densities on semantic segmentation and depth completion tasks, as well as the limitations of current upsampling algorithms for scene-level tasks, and the effect of environmental migration on the robustness of the network in the place recognition task. These findings empirically validate some past conjectures and open new perspectives for developing algorithms with enhanced domain adaptability. The visualization results of some experiments can be found in the supplementary materials.

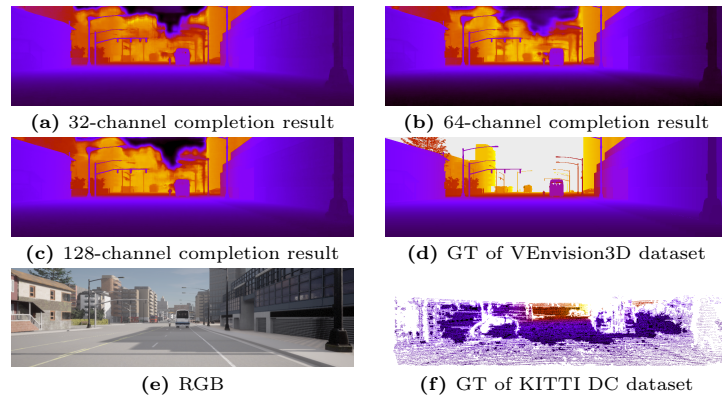


**Fig. 4:** Depth completion results of PENet from different input (32/64/128-channel LiDAR projected image).

**Depth completion.** We carry out experiments on the projected image of different channel count using deep learning methods [24, 42] and traditional methods [70]. Tab. 4 presents our experimental results. PENet achieve the best results, while the other two methods performed poorly. However, it should be noted that

Method	Data <sup>†</sup>	RMSE ↓	MAE ↓
NLSPN [42]	32	6972.50	4482.53
	64	6538.66	4434.13
	128	6021.36	3714.02
	KITTI	741.68	199.59
PENet [24]	32	2833.97	803.90
	64	2808.22	782.92
	128	2724.75	739.43
	KITTI	730.08	210.55
Physical Surface Mod [70]	32	8683.49	5126.70
	64	8405.77	5001.68
	128	8283.88	4950.97
	KITTI	1239.84	298.30

**Table 4:** Benchmarking results of depth completion on the test set. The accuracy are presented as root mean squared error (RMSE [mm]) and mean absolute error (MAE [mm]) <sup>†</sup>We conducted experiments using data of 32/64/128-channel LiDAR point cloud projected image.

Method	Sequence	ATE ↓	ARE ↓
KISS-ICP [59]	Town03	6.399	0.052
	Town05	9.583	0.069
	Town10	3.124	0.022
A-LOAM [67]	Town03	4.514	0.038
	Town05	69.811	0.402
	Town10	3.733	0.034
MULLS [41]	Town03	26.445	0.172
	Town05	228.50	1.221
	Town10	5.224	0.064

**Table 5:** Benchmarking results of LiDAR odometry estimation on each sequence. The errors are presented as absolute trajectory error (ATE [m]) and absolute rotational error (ARE [rad]).

our ground truth was generated by a renderer and is denser than the annotated depth maps in the KITTI DC dataset, so the accuracy of these methods on our dataset is much lower than the results on the KITTI DC dataset. Additionally, we observed that as the LiDAR channel count increased, the accuracy of all methods improve to varying degrees, which was particularly evident in NLSPN. This reveals the limitations of existing methods and demonstrate the enhancing effect of increasing point density on depth completion tasks. Fig. 4 shows the results of PENet for data with different point densities. It can be observed from both quantitative and visual results that with the increase in point density, there is a slight improvement in the accuracy of the completion results.

**LiDAR odometry estimation.** We conduct experiments on three sequences according to the settings of KITTI Odometry. Tab. 5 presents our experimental results, where KISS-ICP [59] achieve the best results in Town05 and Town10, while A-LOAM [67] achieve the best results in Town03. However, it is unusual that MULLS [41] obtain significant deviations in Town03 and Town05, and A-LOAM’s results in Town05 were also unsatisfactory. We also test ORB-SLAM2 [40] using stereo images, but the final performance was poor, as the algorithm lost track early in the sequence. We speculate that the reason for these low accuracy phenomena is due to the sharp turning angle in the trajectories. Overall, KISS-ICP exhibits the strongest robustness, which aligns with its characteristic of not requiring parameter tuning.

**Point cloud place recognition.** Our place recognition dataset use the same data preprocessing procedure as benchmark datasets proposed in [55] (except for removing ground plane points). To investigate the impact of dynamic environments, we generate four sequences before and after simulating environmental changes, denoted as Org. and Mig. respectively. Each run is split into two disjoint reference maps used for training and testing, and each reference map is organized as a set of submaps at regular intervals. We choose PointNetVLAD [55], PPT-



Method	Data <sup>†</sup>	AR@1 $\uparrow$	AR@5 $\uparrow$
PointNetVLAD [55]	Org.	87.7	90.4
	Org.+Mig.	84.3	90.3
PPTNet [28]	Org.	92.6	94.4
	Org.+Mig.	94.1	95.0
MinkLoc3dv2 [32]	Org.	89.9	94.9
	Org.+Mig.	97.1	98.5

**Table 6:** Benchmarking results of place recognition. Average recall at 1(AR@1 [%]) and at 5(AR@5 [%]) are reported. <sup>†</sup>Org.(Original) denotes training that exclusively utilizes data from the original environment, while Org.(Original)+Mig.(Migrated) indicates training that incorporates data from both the original and migrated environments.

Method	Data <sup>†</sup>	CD $\downarrow$	HD $\downarrow$
PC2-PU [38]	16->128	0.255	147.641
	32->128	0.116	74.103
	64->128	0.045	48.572
PU-GCN [43]	16->128	0.124	127.608
	32->128	0.070	64.407
	64->128	0.051	46.531

**Table 7:** Benchmarking results of scene-level point cloud upsampling on the test set. Chamfer distance (CD) and Hausdorff distance (HD) are reported as evaluation metrics. Note that CD and HD are multiplied by  $10^3$ . <sup>†</sup>We use 16/32/64-channel LiDAR scan as input and 128-channel LiDAR scan as ground truth.

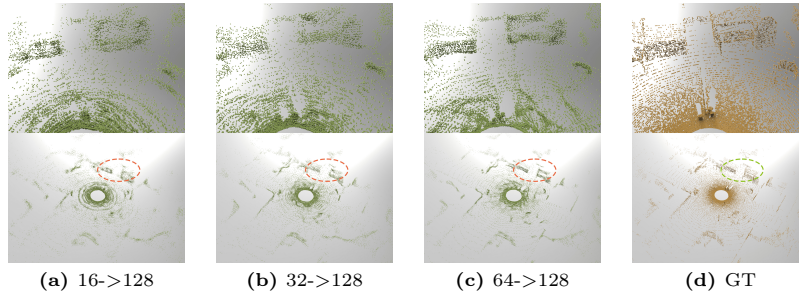


**Fig. 5:** Upsampling results of PU-GCN from different input (16/32/64-channel LiDAR scan). The ground truth is 128-channel LiDAR scan.

Net [28] and MinkLoc3dv2 [32] as global feature extractors for place recognition and train each extractor with 2 different training sets of submaps from Org. only and Org.+Mig. Regarding validation, we uniformly employ cross-validation on all eight sequences. Tab. 6 demonstrated that training PPTNet [28] and MinkLoc3dv2 [32] with two sets of sequence data led to noticeable improvement compared to using only the original sequence. This finding highlights the influence of environmental changes on the accuracy of place recognition for the first time. VEnvision3D datasets can support ongoing research on change-robust or change-aware place recognition techniques. However, concurrent use of both training sets for PointNetVLAD results in a decrease in performance. We conjecture that this is due to the smaller parameter size of the network.

**Scene-level point cloud upsampling.** We conduct upsampling experiments using point-based [43] and transformer-based [38] methods. The results are presented in Tab. 7. It is important to mention that including the HD metric in the evaluation metrics does not effectively reveal the superiority or inferiority of the

Method	Data	mIoU $\uparrow$	car	bicycle	motorcycle	truck	other-vehicle	person	rider	road	sidewalk	ground	building	fence	vegetation	terrain	pole	traffic-sign
Minkowski U-Net [11]	32	69.0	81.8	41.7	51.1	86.1	73.1	60.6	70.3	94.0	75.8	53.4	78.9	80.0	79.5	55.6	57.8	63.9
	64	77.2	90.1	56.2	58.4	92.7	81.6	76.1	79.8	93.0	83.4	64.9	89.4	88.0	90.7	57.7	63.5	68.9
	128	82.9	95.0	73.9	76.4	95.0	76.3	84.3	82.3	93.5	86.6	63.9	95.8	93.6	95.9	60.0	80.3	73.4
RandLA-Net [26]	32	60.2	49.1	24.0	35.3	91.3	33.8	26.6	18.4	97.0	88.8	63.5	94.3	88.9	92.5	78.6	81.0	0.0
	64	69.5	66.9	26.0	53.0	96.7	82.2	56.6	1.8	98.4	92.0	73.0	97.5	94.2	96.6	87.7	89.0	0.0
	128	73.2	71.0	34.1	59.2	96.9	81.7	68.8	31.0	98.5	92.3	68.2	97.6	94.9	97.1	88.3	91.5	0.0
KPConv [53]	32	62.3	90.7	42.0	48.9	82.8	1.4	73.5	65.9	90.8	73.3	8.6	80.0	63.7	86.9	43.5	71.2	72.9
	64	76.2	95.8	64.1	65.5	91.4	27.7	84.4	76.8	92.8	80.4	49.7	91.8	87.9	94.4	53.3	80.5	82.7
	128	77.7	92.7	68.7	67.6	96.0	90.7	87.8	79.7	90.8	74.7	32.7	88.2	83.3	96.3	41.3	73.8	79.3

**Table 8:** Benchmarking results of point cloud semantic segmentation on the validation set. We conducted experiments on data with different point densities. Mean IoU (mIoU [%]), and per-class IoU [%] scores are reported.

algorithm in scene-level upsampling experiments since HD only reflects the maximum mismatch between point sets. As can be seen, PU-GCN performs better in 16/32-channel input while PC2-PU is better in 64-channel input. As the density of input points increases, the accuracy of prediction results also improves. This characteristic is more prominent in PC2-PU. The specific visual results are shown in Fig. 5. For the first time, we complete the evaluation of the upsampling task on scene-level point clouds. However, from this result, it can also be seen that compared to traditional 3D object upsampling tasks, the upsampling effect at the scene level is not satisfactory. The details of some large buildings are severely lost, which poses new challenges for the point cloud upsampling task.

**Point cloud semantic segmentaion.** We utilize pointwise-MLP-based [26], point-convolution-based [53] and voxel-based [11] methods to test our dataset. The results are shown in Tab. 8. It can be seen that point-convolution-based Minkowski U-Net achieve the best results(voxel size is all set to 0.05). As for the pointwise-MLP-based RandLA-Net, the test results for different channel count are not satisfactory. For example, for small categories like traffic signs, there are even cases where the IoU is 0. We speculate that this is because the downsampling strategy used in RandLA-Net is not suitable for segmenting small objects in large scenes, resulting in performance degradation. In point-convolution-based KPConv, compared to the 64-channel data, the 128-channel data did not show a significant improvement. This is because, for the KPConv, with higher-density input point clouds, precise adjustment of the neighborhood radius is essential to prevent performance degradation. The multi-density point clouds we offer facilitate robustness testing of semantic segmentation algorithms across domains, aiding researchers in exploring domain adaptation or generalization studies.

## 5 Multi-task Exploration

In this section, we take upsampling and segmentation as examples to investigate the mutual reinforcement between different tasks. The experimental results show that there is indeed a mutually reinforcing effect between the two subtasks, and that simultaneous training accelerates convergence and improves performance. This also partially demonstrates that our dataset can facilitate 3D multitasking research and represents more possibilities for the future research.

### 5.1 The Network

We adopt PU-Dense [2] network architecture as the backbone network and extend a branch for semantic segmentation task. The detailed network architecture is illustrated in Fig. 6. Apart from the original PU-Dense structure, we incorporate transposed convolution [11] to upsample features from different scales of the encoder. These features are then concatenated as input, and the SENet [22] is applied to learn the importance of each channel. Ultimately, a linear classifier is employed to accomplish the semantic segmentation. Besides, we adjust the expansion factor (kernel size) for coordinate generation within the PU-Dense network to accommodate large-scale scenes.

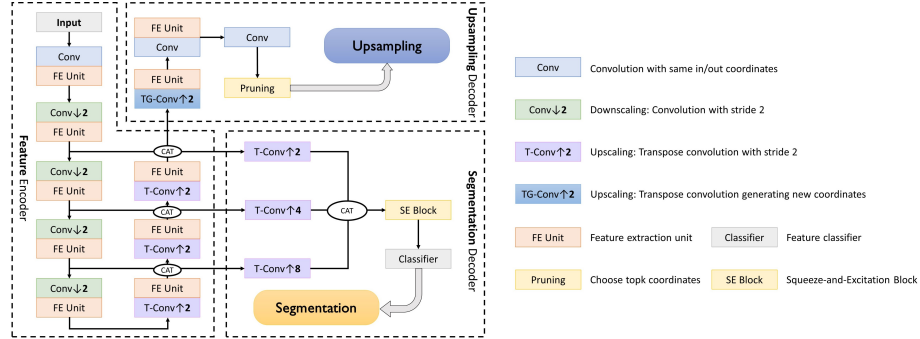


**Fig. 6:** Multi-task end-to-end network architecture. We adopt PU-Dense as the backbone network architecture and expand it with a semantic segmentation branch.

### 5.2 Loss Function

For the upsampling branch, we employ a voxel-based BCE Loss consistent with PU-Dense, while for the semantic segmentation branch, we use the conventional CE Loss. The final loss for the entire network is the average of these values, with the detailed definition as follows:

$$\mathcal{L}_{BCE} = -\frac{1}{N} \sum_i (x_i \log(p_i) + (1 - x_i) \log(1 - p_i)) \quad (1)$$

$$\mathcal{L}_{CE} = -\frac{1}{N} \sum_i x_i \log(p_i) \quad (2)$$

$$\mathcal{L} = \frac{1}{2} \mathcal{L}_{BCE} + \frac{1}{2} \mathcal{L}_{CE} \quad (3)$$

In  $\mathcal{L}_{BCE}$ ,  $x_i$  is the voxel label that is either occupied (1) or empty (0) in the GT point cloud.  $p_i$  is the probability of the voxel being occupied and is calculated using a *sigmoid* function applied to the decoder output  $D_0$ . In  $\mathcal{L}_{CE}$ ,  $x_i$  refers to the one-hot label entry, and  $p_i$  represents the probability of a point being predicted as a certain class.

### 5.3 Experiments

To explore the relationships between multiple sub-tasks, we adopt the following experimental strategies: training solely with the upsampling branch; training solely with the semantic segmentation branch; and simultaneous training with both the upsampling and semantic segmentation branches. Such a design allows us to quantify the phenomena of inter-task influence, providing a research basis for the design of end-to-end foundation models.

Using data with different point densities from our dataset, we take the coordinate values of the 32-channel point cloud as input, the 128-channel point cloud as the ground truth for upsampling, and the label values of the 32-channel point cloud as the ground truth for semantic segmentation. For a fair comparison, the Adam [30] and SGD [48] optimizer is used with a weight decay of 0.0001 and a default learning rate of 0.002. We use exponentialLR [35] to adjust learning rate and the gamma is 0.5. During the training procedure, random rotation along z-axis is performed for the augmentation. The model is trained for 5 epochs with a batch size of 4 under each setting.

Branch	Ups. AR $\uparrow$	Ups. CD $\downarrow$	Seg. mIoU $\uparrow$
Ups.	43.2	45.5	-
Seg.	-	-	43.6
<b>Ups+Seg.</b>	<b>46.5</b>	<b>43.1</b>	<b>45.3</b>

**Table 9:** We conduct experiments on the upsampling branch(Ups.), the semantic segmentation branch(Seg.), and both branches simultaneously(Ups.+Seg.). Chamfer distance(CD, multiplied by  $10^3$ ) and average recall(AR [%]) is reported as evaluation metrics for upsamplig and mean IOU(mIoU [%]) is reported for semantic segmentation.

The experimental results are shown in Tab. 9. From the experimental results, it can be observed that when the upsampling and segmentation branches are conducted simultaneously, both the Average Recall (AR) of the upsampling task and the mean Intersection over Union (mIoU) of the segmentation task show

improvement. They increase from 43.2% to 46.5% and from 43.6% to 45.3%, respectively. Such results demonstrate the phenomenon of mutual promotion among specific downstream sub-tasks. The upsampling task forces the encoder to capture the implicit surface structure of objects, and such information can provide geometric constraints for semantic segmentation. Conversely, the semantic information provided by the semantic segmentation task can also assist the upsampling task in obtaining category-related information, thereby improving the upsampling process.

It is worth noting that the Chamfer Distance (CD) does not meet the expected performance as PU-Dense is a voxel-based method that achieves upsampling by expanding the voxels occupied by the original spatial points. So it does not adequately reflect the quality of the upsampling.

Through simple experimental setups, we can preliminarily leverage the proposed dataset for multi-task learning. This demonstrates the advantage of collecting the dataset from the same scenarios, allowing for the convenient integration of multiple tasks without the need for complex mappings. This also reflects that our dataset can support the exploration of the future end-to-end framework.

## 6 Discussion and Conclusion

We introduce VEnvision3D, a synthetic perception dataset featuring the exploration of 3D multi-task models, including depth completion, segmentation, upsampling, place recognition, and 3D reconstruction. In a virtual environment, we implement innovative sensor configurations, endowing our dataset with unique characteristics. For instance, it can provide data with varying densities within the same frame, offer surface-sampled data at a city level, and simulate environmental changes. These features aim to contribute to the advancement of the field of point cloud perception. In addition, benefiting from the carefully designed settings in our data collection, we integrate the upsampling task and semantic segmentation task into a multi-task framework. Through experiments, we preliminarily demonstrate the mutually beneficial relationship among different sub-tasks.

However, we also acknowledge the limitations of our dataset. Joint training with only two subtasks can only provide preliminary evidence of the relevance of certain 3D perception tasks. To achieve a truly multi-task end-to-end network, further effective experiments and explorations are needed. We plan to progressively incorporate more sub-tasks in the future to continue our research.

Additionally, although virtual environments possess unique advantages, one might argue that the domain gap between synthetic and real data is a weakness. In our defense, we believe that when synthetic data is used correctly, it can be used to enhance task performance on real data. For example, [14] indicates that the dataset generated by the CARLA simulator can improve the accuracy of point cloud semantic segmentation to a certain extent. [49] showed that augmenting with point clouds generated from Carla simulator can improve bird’s eye view 2D detection performance on the real-world KITTI dataset. [16, 25, 62]

developed several domain adaptation methods to mitigate domain shift as much as possible. Furthermore, we also adjusted the sensor settings and added noise on LiDAR to minimize domain shift as much as possible.

In summary, by introducing VEnvision3D, hope that our dataset can aid researchers in conducting more novel preliminary explorations under the current scarcity of 3D datasets, to better realize more grounded concepts in the future. We believe our work is a valuable and necessary first step towards 3D multi-task learning and deserves sharing with the community.

## References

1. Papers with code. <https://paperswithcode.com/> **2**
2. Akhtar, A., Li, Z., Van der Auwera, G., Li, L., Chen, J.: Pu-dense: Sparse tensor-based point cloud geometry upsampling. *IEEE Transactions on Image Processing* **31**, 4133–4148 (2022) **13**
3. Armeni, I., Sax, A., Zamir, A.R., Savarese, S.: Joint 2D-3D-Semantic Data for Indoor Scene Understanding. *ArXiv e-prints* (Feb 2017) **2, 4**
4. Behley, J., Garbade, M., Milioto, A., Quenzel, J., Behnke, S., Stachniss, C., Gall, J.: SemanticKITTI: A Dataset for Semantic Scene Understanding of LiDAR Sequences. In: *Proc. of the IEEE/CVF International Conf. on Computer Vision (ICCV)* (2019) **2, 4, 6**
5. Bogo, F., Romero, J., Loper, M., Black, M.J.: Faust: Dataset and evaluation for 3d mesh registration. In: *Proceedings of the IEEE conference on computer vision and pattern recognition*. pp. 3794–3801 (2014) **4**
6. Bommasani, R., Hudson, D.A., Adeli, E., Altman, R., Arora, S., von Arx, S., Bernstein, M.S., Bohg, J., Bosselut, A., Brunskill, E., et al.: On the opportunities and risks of foundation models. *arXiv preprint arXiv:2108.07258* (2021) **1**
7. Can, G., Mantegazza, D., Abbate, G., Chappuis, S., Giusti, A.: Semantic segmentation on swiss3dcities: A benchmark study on aerial photogrammetric 3d pointcloud dataset. *Pattern Recognition Letters* **150**, 108–114 (2021) **4**
8. Carlevaris-Bianco, N., Ushani, A.K., Eustice, R.M.: University of Michigan North Campus long-term vision and lidar dataset. *International Journal of Robotics Research* **35**(9), 1023–1035 (2015) **5**
9. Chang, A.X., Funkhouser, T., Guibas, L., Hanrahan, P., Huang, Q., Li, Z., Savarese, S., Savva, M., Song, S., Su, H., Xiao, J., Yi, L., Yu, F.: ShapeNet: An Information-Rich 3D Model Repository. *Tech. Rep. arXiv:1512.03012 [cs.GR]*, Stanford University — Princeton University — Toyota Technological Institute at Chicago (2015) **2, 4**
10. Chen, M., Hu, Q., Yu, Z., THOMAS, H., Feng, A., Hou, Y., McCullough, K., Ren, F., Soibelman, L.: Stpls3d: A large-scale synthetic and real aerial photogrammetry 3d point cloud dataset. In: *33rd British Machine Vision Conference 2022, BMVC 2022, London, UK, November 21-24, 2022. BMVA Press* (2022), <https://bmvc2022.mpi-inf.mpg.de/0429.pdf> **2, 5**
11. Choy, C., Gwak, J., Savarese, S.: 4d spatio-temporal convnets: Minkowski convolutional neural networks. In: *Proceedings of the IEEE Conference on Computer Vision and Pattern Recognition*. pp. 3075–3084 (2019) **12, 13**
12. Deng, J., Dong, W., Socher, R., Li, L.J., Li, K., Fei-Fei, L.: Imagenet: A large-scale hierarchical image database. In: *2009 IEEE conference on computer vision and pattern recognition*. pp. 248–255. Ieee (2009) **2**



13. Deschaud, J.E.: KITTI-CARLA: a KITTI-like dataset generated by CARLA Simulator. arXiv e-prints arXiv:2109.00892 (2021) [2](#), [5](#)
14. Deschaud, J.E., Duque, D., Richa, J.P., Velasco-Forero, S., Marcotegui, B., Goulette, F.: Paris-carla-3d: A real and synthetic outdoor point cloud dataset for challenging tasks in 3d mapping. *Remote Sensing* **13**(22), 4713 (2021) [5](#), [15](#)
15. Dosovitskiy, A., Ros, G., Codevilla, F., Lopez, A., Koltun, V.: CARLA: An open urban driving simulator. In: *Proceedings of the 1st Annual Conference on Robot Learning*. pp. 1–16 (2017) [3](#), [4](#)
16. Espadinha, J., Lebedev, I., Lukic, L., Bernardino, A.: Lidar data noise models and methodology for sim-to-real domain generalization and adaptation in autonomous driving perception. In: *2021 IEEE Intelligent Vehicles Symposium (IV)*. pp. 797–803. IEEE (2021) [15](#)
17. Geiger, A., Lenz, P., Stiller, C., Urtasun, R.: Vision meets robotics: The kitti dataset. *International Journal of Robotics Research (IJRR)* (2013) [2](#), [5](#), [6](#), [8](#)
18. Griffiths, D., Boehm, J.: SynthCity: A large scale synthetic point cloud. In: *ArXiv preprint* (2019) [2](#), [4](#)
19. Hackel, T., Savinov, N., Ladicky, L., Wegner, J.D., Schindler, K., Pollefeys, M.: SEMANTIC3D.NET: A new large-scale point cloud classification benchmark. In: *ISPRS Annals of the Photogrammetry, Remote Sensing and Spatial Information Sciences*. vol. IV-1-W1, pp. 91–98 (2017) [4](#)
20. Hastings, W.K.: *Monte carlo sampling methods using markov chains and their applications* (1970) [7](#)
21. Hsu, L.T., Kubo, N., Wen, W., Chen, W., Liu, Z., Suzuki, T., Meguro, J.: Urbannav: An open-sourced multisensory dataset for benchmarking positioning algorithms designed for urban areas. In: *Proceedings of the 34th International Technical Meeting of the Satellite Division of The Institute of Navigation (ION GNSS+ 2021)*. pp. 226–256 (2021) [5](#)
22. Hu, J., Shen, L., Sun, G.: *Squeeze-and-excitation networks* (2018) [13](#)
23. Hu, J., Bao, C., Ozay, M., Fan, C., Gao, Q., Liu, H., Lam, T.L.: Deep depth completion from extremely sparse data: A survey. *IEEE Transactions on Pattern Analysis and Machine Intelligence* (2022) [4](#)
24. Hu, M., Wang, S., Li, B., Ning, S., Fan, L., Gong, X.: Towards precise and efficient image guided depth completion (2021) [9](#), [10](#)
25. Hu, Q., Yang, B., Khalid, S., Xiao, W., Trigoni, N., Markham, A.: Towards semantic segmentation of urban-scale 3d point clouds: A dataset, benchmarks and challenges. In: *Proceedings of the IEEE/CVF Conference on Computer Vision and Pattern Recognition* (2021) [4](#), [15](#)
26. Hu, Q., Yang, B., Xie, L., Rosa, S., Guo, Y., Wang, Z., Trigoni, N., Markham, A.: Randla-net: Efficient semantic segmentation of large-scale point clouds. *Proceedings of the IEEE Conference on Computer Vision and Pattern Recognition* (2020) [12](#)
27. Hu, Y., Yang, J., Chen, L., Li, K., Sima, C., Zhu, X., Chai, S., Du, S., Lin, T., Wang, W., et al.: Planning-oriented autonomous driving. In: *Proceedings of the IEEE/CVF Conference on Computer Vision and Pattern Recognition*. pp. 17853–17862 (2023) [1](#)
28. Hui, L., Yang, H., Cheng, M., Xie, J., Yang, J.: Pyramid point cloud transformer for large-scale place recognition. In: *ICCV* (2021) [11](#)
29. Kim, G., Park, Y.S., Cho, Y., Jeong, J., Kim, A.: Mulran: Multimodal range dataset for urban place recognition. In: *Proceedings of the IEEE International Conference on Robotics and Automation (ICRA)*. Paris (May 2020) [5](#)

30. Kingma, D.P., Ba, J.: Adam: A method for stochastic optimization. arXiv preprint arXiv:1412.6980 (2014) [14](#)
31. Kirillov, A., Mintun, E., Ravi, N., Mao, H., Rolland, C., Gustafson, L., Xiao, T., Whitehead, S., Berg, A.C., Lo, W.Y., Dollár, P., Girshick, R.: Segment anything. arXiv:2304.02643 (2023) [1](#)
32. Komorowski, J.: Improving point cloud based place recognition with ranking-based loss and large batch training. In: 2022 26th International Conference on Pattern Recognition (ICPR). pp. 3699–3705 (2022). <https://doi.org/10.1109/ICPR56361.2022.9956458> [11](#)
33. Li, R., Li, X., Fu, C.W., Cohen-Or, D., Heng, P.A.: Pu-gan: a point cloud upsampling adversarial network. In: Proceedings of the IEEE/CVF international conference on computer vision. pp. 7203–7212 (2019) [4](#)
34. Li, X., Li, C., Tong, Z., Lim, A., Yuan, J., Wu, Y., Tang, J., Huang, R.: Campus3d: A photogrammetry point cloud benchmark for hierarchical understanding of outdoor scene. In: Proceedings of the 28th ACM International Conference on Multimedia. pp. 238–246 (2020) [4](#)
35. Li, Z., Arora, S.: An exponential learning rate schedule for deep learning. arXiv preprint arXiv:1910.07454 (2019) [14](#)
36. Lin, T.Y., Maire, M., Belongie, S., Hays, J., Perona, P., Ramanan, D., Dollár, P., Zitnick, C.L.: Microsoft coco: Common objects in context. In: Computer Vision—ECCV 2014: 13th European Conference, Zurich, Switzerland, September 6–12, 2014, Proceedings, Part V 13. pp. 740–755. Springer (2014) [2](#)
37. Liu, Z., Luo, P., Wang, X., Tang, X.: Deep learning face attributes in the wild. In: Proceedings of International Conference on Computer Vision (ICCV) (December 2015) [2](#)
38. Long, C., Zhang, W., Li, R., Wang, H., Dong, Z., Yang, B.: Pc2-pu: Patch correlation and point correlation for effective point cloud upsampling. In: Proceedings of the 30th ACM International Conference on Multimedia. pp. 2191–2201 (2022) [11](#)
39. Maddern, W., Pascoe, G., Linegar, C., Newman, P.: 1 Year, 1000km: The Oxford RobotCar Dataset. The International Journal of Robotics Research (IJRR) **36**(1), 3–15 (2017). <https://doi.org/10.1177/0278364916679498>, <http://dx.doi.org/10.1177/0278364916679498> [2](#), [5](#), [6](#)
40. Mur-Artal, R., Tardós, J.D.: ORB-SLAM2: an open-source SLAM system for monocular, stereo and RGB-D cameras. IEEE Transactions on Robotics **33**(5), 1255–1262 (2017). <https://doi.org/10.1109/TR0.2017.2705103> [10](#)
41. Pan, Y., Xiao, P., He, Y., Shao, Z., Li, Z.: Mulls: Versatile lidar slam via multi-metric linear least square. In: 2021 IEEE International Conference on Robotics and Automation (ICRA). pp. 11633–11640. IEEE (2021) [10](#)
42. Park, J., Joo, K., Hu, Z., Liu, C.K., Kweon, I.S.: Non-local spatial propagation network for depth completion. In: Proc. of European Conference on Computer Vision (ECCV) (2020) [9](#), [10](#)
43. Qian, G., Abualshour, A., Li, G., Thabet, A., Ghanem, B.: Pu-gcn: Point cloud upsampling using graph convolutional networks. In: Proceedings of the IEEE/CVF Conference on Computer Vision and Pattern Recognition (CVPR). pp. 11683–11692 (June 2021) [4](#), [11](#)
44. Qian, Y., Hou, J., Kwong, S., He, Y.: Pugeo-net: A geometry-centric network for 3d point cloud upsampling. In: European conference on computer vision. pp. 752–769. Springer (2020) [4](#)
45. Qiu, J., Cui, Z., Zhang, Y., Zhang, X., Liu, S., Zeng, B., Pollefeys, M.: Deeplidar: Deep surface normal guided depth prediction for outdoor scene from sparse lidar

- data and single color image. In: The IEEE Conference on Computer Vision and Pattern Recognition (CVPR) (June 2019) [4](#)
46. Radford, A., Kim, J.W., Hallacy, C., Ramesh, A., Goh, G., Agarwal, S., Sastry, G., Askell, A., Mishkin, P., Clark, J., et al.: Learning transferable visual models from natural language supervision. In: International conference on machine learning. pp. 8748–8763. PMLR (2021) [1](#)
  47. Roynard, X., Deschaud, J.E., Goulette, F.: Paris-lille-3d: A large and high-quality ground-truth urban point cloud dataset for automatic segmentation and classification. *The International Journal of Robotics Research* **37**(6), 545–557 (2018). <https://doi.org/10.1177/0278364918767506> [4](#)
  48. Ruder, S.: An overview of gradient descent optimization algorithms. arXiv preprint arXiv:1609.04747 (2016) [14](#)
  49. Sallab, A., Sobh, I., Zahran, M., Shawky, M.: Unsupervised neural sensor models for synthetic lidar data augmentation. arXiv: Computer Vision and Pattern Recognition, arXiv: Computer Vision and Pattern Recognition (Nov 2019) [15](#)
  50. Serna, A., Marcotegui, B., Goulette, F., Deschaud, J.E.: Paris-rue-madame database: a 3d mobile laser scanner dataset for benchmarking urban detection, segmentation and classification methods. In: 4th international conference on pattern recognition, applications and methods ICPRAM 2014 (2014) [4](#)
  51. Singer, N.M., Asari, V.K.: Dales objects: A large scale benchmark dataset for instance segmentation in aerial lidar. *IEEE Access* pp. 1–1 (2021). <https://doi.org/10.1109/ACCESS.2021.3094127> [4](#)
  52. Sun, T., Segu, M., Postels, J., Wang, Y., Van Gool, L., Schiele, B., Tombari, F., Yu, F.: SHIFT: a synthetic driving dataset for continuous multi-task domain adaptation. In: Proceedings of the IEEE/CVF Conference on Computer Vision and Pattern Recognition (CVPR). pp. 21371–21382 (June 2022) [2](#), [5](#)
  53. Thomas, H., Qi, C.R., Deschaud, J.E., Marcotegui, B., Goulette, F., Guibas, L.J.: Kpconv: Flexible and deformable convolution for point clouds. *Proceedings of the IEEE International Conference on Computer Vision* (2019) [12](#)
  54. Uhrig, J., Schneider, N., Schneider, L., Franke, U., Brox, T., Geiger, A.: Sparsity invariant cnns. In: International Conference on 3D Vision (3DV) (2017) [3](#), [6](#)
  55. Uy, M.A., Lee, G.H.: Pointnetvlad: Deep point cloud based retrieval for large-scale place recognition. In: The IEEE Conference on Computer Vision and Pattern Recognition (CVPR) (2018) [10](#), [11](#)
  56. Uy, M.A., Pham, Q.H., Hua, B.S., Nguyen, D.T., Yeung, S.K.: Revisiting point cloud classification: A new benchmark dataset and classification model on real-world data. In: International Conference on Computer Vision (ICCV) (2019) [4](#)
  57. Vafaeikia, P., Namdar, K., Khalvati, F.: A brief review of deep multi-task learning and auxiliary task learning. arXiv preprint arXiv:2007.01126 (2020) [2](#)
  58. Vallet, B., Brédif, M., Serna, A., Marcotegui, B., Paparoditis, N.: Terramobilita/iqmulus urban point cloud analysis benchmark. *Computers & Graphics* **49**, 126–133 (2015) [4](#)
  59. Vizzo, I., Guadagnino, T., Mersch, B., Wiesmann, L., Behley, J., Stachniss, C.: KISS-ICP: In Defense of Point-to-Point ICP – Simple, Accurate, and Robust Registration If Done the Right Way. *IEEE Robotics and Automation Letters (RA-L)* **8**(2), 1029–1036 (2023). <https://doi.org/10.1109/LRA.2023.3236571> [10](#)
  60. Weng, X., Man, Y., Park, J., Yuan, Y., Cheng, D., O’Toole, M., Kitani, K.: All-In-One Drive: A Large-Scale Comprehensive Perception Dataset with High-Density Long-Range Point Clouds. arXiv (2021) [2](#), [5](#)

61. Wu, Z., Song, S., Khosla, A., Yu, F., Zhang, L., Tang, X., Xiao, J.: 3d shapenets: A deep representation for volumetric shapes. In: Proceedings of the IEEE conference on computer vision and pattern recognition. pp. 1912–1920 (2015) [4](#)
62. Xiao, A., Huang, J., Guan, D., Zhan, F., Lu, S.: Transfer learning from synthetic to real lidar point cloud for semantic segmentation. In: Proceedings of the AAAI Conference on Artificial Intelligence. vol. 36, pp. 2795–2803 (2022) [5](#), [15](#)
63. Ye, Z., Xu, Y., Huang, R., Tong, X., Li, X., Liu, X., Luan, K., Hoegner, L., Stilla, U.: Lasdu: A large-scale aerial lidar dataset for semantic labeling in dense urban areas. *ISPRS International Journal of Geo-Information* **9**(7), 450 (2020) [4](#)
64. Yu, L., Li, X., Fu, C.W., Cohen-Or, D., Heng, P.A.: Ec-net: an edge-aware point set consolidation network. In: Proceedings of the European conference on computer vision (ECCV). pp. 386–402 (2018) [4](#)
65. Yu, L., Li, X., Fu, C.W., Cohen-Or, D., Heng, P.A.: Pu-net: Point cloud upsampling network. In: Proceedings of the IEEE conference on computer vision and pattern recognition. pp. 2790–2799 (2018) [4](#)
66. Yu, Q., Chu, L., Wu, Q., Pei, L.: Grayscale and normal guided depth completion with a low-cost lidar. In: 2021 IEEE International Conference on Image Processing (ICIP). pp. 979–983. IEEE (2021) [4](#)
67. Zhang, J., Singh, S.: Loam: Lidar odometry and mapping in real-time. In: Robotics: Science and systems. vol. 2, pp. 1–9. Berkeley, CA (2014) [10](#)
68. Zhang, Y., Yang, Q.: An overview of multi-task learning. *National Science Review* **5**(1), 30–43 (2018) [2](#)
69. Zhao, W.X., Zhou, K., Li, J., Tang, T., Wang, X., Hou, Y., Min, Y., Zhang, B., Zhang, J., Dong, Z., et al.: A survey of large language models. *arXiv preprint arXiv:2303.18223* (2023) [2](#)
70. Zhao, Y., Bai, L., Zhang, Z., Huang, X.: A surface geometry model for lidar depth completion. *IEEE Robotics and Automation Letters* **6**(3), 4457–4464 (2021) [9](#), [10](#)
71. Zolanvari, S., Ruano, S., Rana, A., Cummins, A., da Silva, R.E., Rahbar, M., Smolic, A.: Dublincity: Annotated lidar point cloud and its applications. *arXiv preprint arXiv:1909.03613* (2019) [4](#)

## 7 Supplementary Material

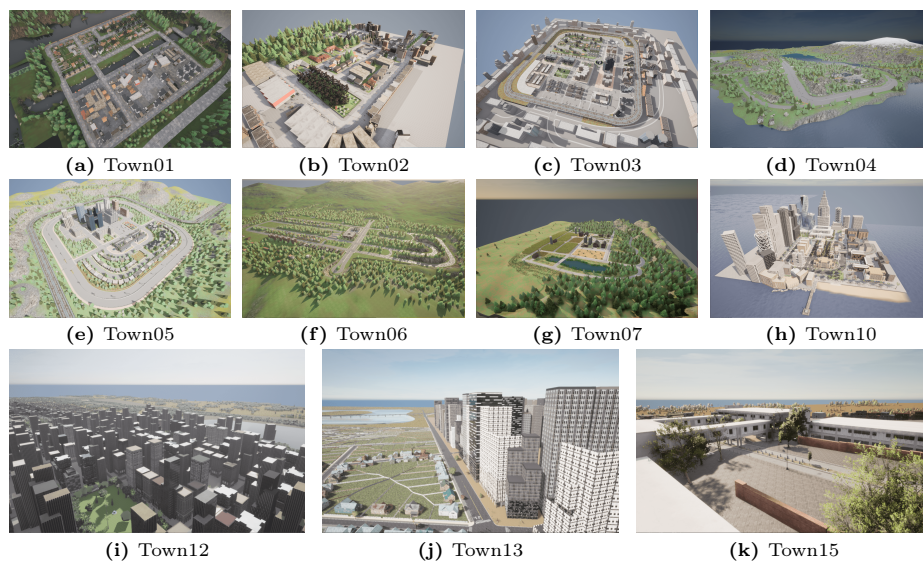


**Fig. 7:** The 11 city maps used during the collection process.

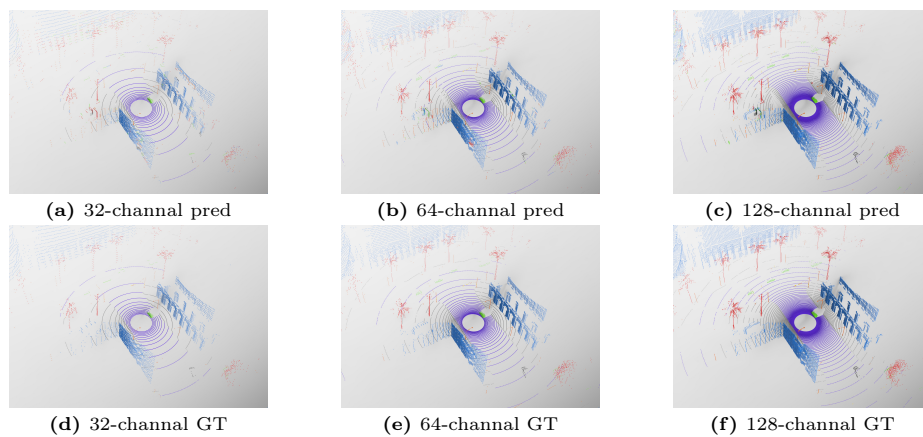


**Fig. 8:** Semantic segmentation results of Minkowski U-Net from different input (32/64/128-channel LiDAR scan).

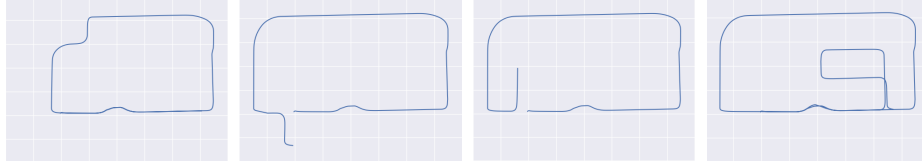


**Fig. 9:** Visualization results of the designed 4 routes in point cloud place recognition task.

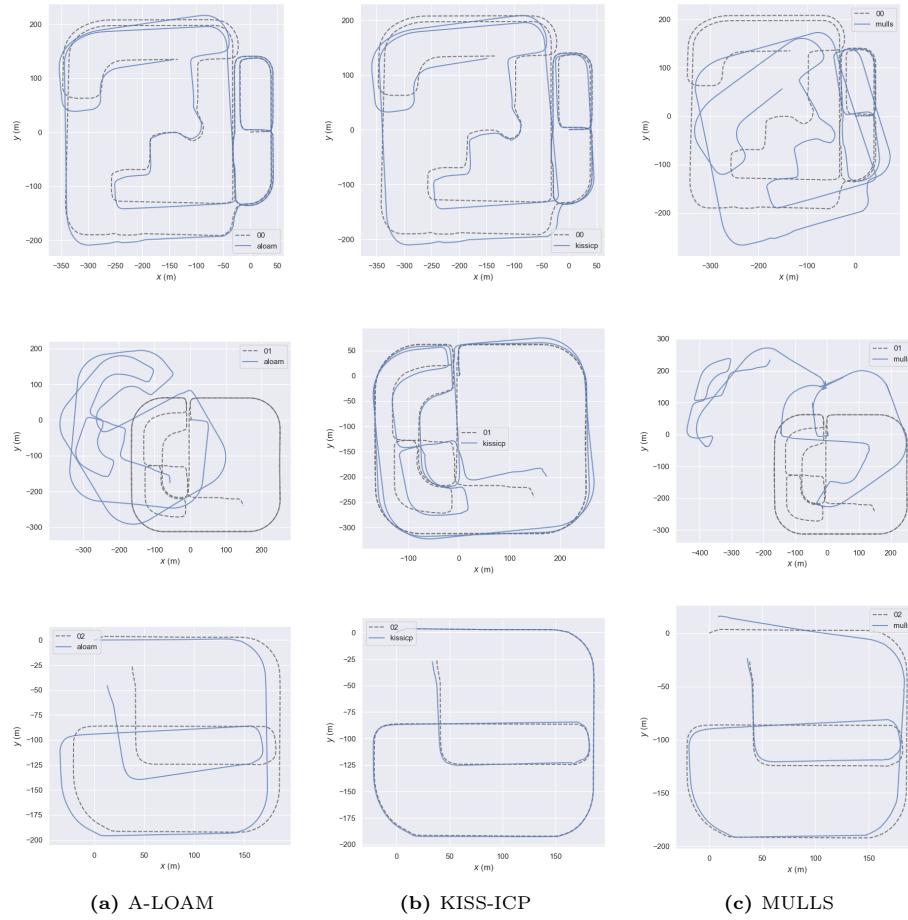


**Fig. 10:** Visualization results of LiDAR odometry estimation on each sequence. Note that 00 refers to sequence Town03, 01 refers to sequence Town05 and 02 refers to sequence Town10.